Miner Petrol (2009) 96:163–175
DOI 10.1007/s00710-009-0058-1

ORIGINAL PAPER

From emplacement to unroofing: thermal history of the Jiazishan gabbro, Sulu UHP terrane, China

W. Siebel · M. Danišík · F. Chen

Received: 3 February 2009 / Accepted: 1 May 2009 / Published online: 15 May 2009

Abstract On the eastern extremity of the Jiaodong peninsula, China, shoshonitic magmas have been injected into the supracrustal rocks of the Sulu ultra-high pressure (UHP) terrane during the crustal exhumation phase. These granitoids (collectively termed the Shidao igneous complex or Jiazishan alkaline complex) show geochemical and isotopic signatures of an enriched subcontinental lithospheric mantle and intruded soon after the subducted Yangtze crust had reached peak metamorphic pressure conditions (240–220 Ma). We have applied various geochronometers to an alkali-gabbro sample from the Jiazishan pluton and the results allow reconstruction of the Triassic-to-present thermal history. Initial rapid cooling of the gabbro at crustal depths is indicated by the close agreement between the Sm-Nd mineral isochron age (228±36 Ma) and the Rb-Sr biotite age (207±1) Ma. This interpretation is confirmed by previously published U-Pb zircon ages (225–209 Ma), and $^{40}Ar/^{39}Ar$ amphibole and K-feldspar ages (~214 Ma) from the Jiazishan syenites. A titanite fission-track age of 166±8 Ma (closure temperature range 285–240°C) records widespread Jurassic magmatism in the Jiaodong peninsula, indicating that the gabbro reached upper crustal levels before it was reheated by nearby Jurassic plutons. A subsequent cooling and reheating event is indicated by an apatite fission-track age of 106±6 Ma which coincides with the emplacement of the adjacent Weideshan pluton (108±2 Ma) and postdates a period of regional lithospheric thinning beneath eastern China. A period of slow cooling (or thermal stability) from late Cretaceous to early Tertiary, documented by an apatite (U-Th)/He age of 39±5 Ma, was followed by a final stage of more enhanced cooling since the late Eocene. Results of this work imply that the eastern Sulu terrane has experienced a complex cooling and reheating history. Our data are consistent with a model of initial rapid cooling (sudden exhumation) of the UHP terrane, driven by the release of buoyancy forces, followed by two progressively slower cooling intervals (both after renewed crustal reheating) during the Jurassic and Cretaceous.

Editorial handling: G. Hoinkes

W. Siebel (✉) · M. Danišík
Institute of Geosciences, University of Tübingen,
72074 Tübingen, Germany
e-mail: wolfgang.siebel@uni-tuebingen.de

M. Danišík
John de Laeter Centre of Mass Spectrometry,
Department of Applied Geology,
Curtin University of Technology,
Perth, WA 6845, Australia

F. Chen
Key Laboratory of Mineral Resources,
Institute of Geology and Geophysics,
Chinese Academy of Sciences,
100029 Beijing, China

F. Chen
Key Laboratory of Crust-Mantle Materials and Environments,
School of Earth Sciences, University of Science and Technology,
230026 Hefei, China

Introduction

The Dabie-Sulu orogen in central and eastern China contains the largest accumulation of ultra-high pressure (UHP) rocks on Earth (for a review see Zheng et al. 2003). These rocks formed when continental crust of the Yangtze plate was subducted below the North China craton. Since initial reports of coesite (Okay et al. 1989; Wang et al. 1989) and micro-diamond (Xu et al. 1992) in eclogites,

much effort has been made to obtain time constraints on UHP metamorphism (e.g. Ames et al. 1993; Li et al. 1993, 1999a, 2000; Ayers et al. 2002) and the presently existing radiometric data set (U-Pb, Sm-Nd, Ar-Ar) suggests a middle-Triassic (240–220 Ma) age for this event.

The magmatic record indicates that pre- and syn-collisional granitoids are absent in the Dabie-Sulu belt. No magmatic arc has been identified, leading to the general assumption that arc magmas have either been completely eroded (Webb et al. 1999) or did not develop during subduction due to insufficient release of water-rich fluids from the subducted supracrustal rocks (Zheng et al. 2003). Moreover, post-collisional magmatic rocks of Triassic age are largely absent in the Dabie-Sulu belt, in contrast to the UHP-free Qinling belt, central China, where such rocks have been identified (Sun et al. 2002). However, Lin et al. (1992) reported a Triassic Rb-Sr age from igneous rocks in the eastern extremity of the Sulu UHP terrane. Recently this age was confirmed by U-Pb zircon TIMS and SHRIMP analyses (Chen et al. 2003; Guo et al. 2005; Yang et al. 2005) and a syn-exhumational tectonic genesis of these rocks, known as *Shidao igneous complex* (Chen et al. 2003) or *Jiazishan alkaline complex* (Yang et al. 2005), was proposed.

Granitoids from the Shidao igneous complex do not only provide an excellent opportunity to study subcontinental mantle enrichment processes (Gao et al. 2004; Yang et al. 2005), they also allow constraints to be placed on the thermal history during exhumation of the subducted continental slab. Whereas it is well documented that the first phase of UHP rock exhumation, from mantle to crustal depths, was very rapid (Li et al. 2000; Liu et al. 2006, 2007; Zhao et al. 2006), the later thermal history is less well constrained. In this study we report radiogenic and stable isotope data and fission-track and (U-Th)/He ages for various minerals from an alkali-gabbro from the Shidao igneous complex which help to unravel the formation, cooling and uplift history of this complex.

Geological setting

The Qinling-(Tongbai)-Dabie-Sulu orogenic belt of East Asia was formed by collision between the North China and Yangtze cratons after the closure of an intervening oceanic basin during the Permo-Triassic (for a recent review, see Ernst et al. 2007). The well-studied Dabie-Sulu portion represents the eastern segment of this belt. The high pressure (HP) and UHP rocks of this belt formed in response to deep subduction within a northward dipping subduction zone.

The Sulu terrane is offset from the Dabie terrane by the Tan-Lu fault and bounded by the Wulian–Qingdao–Yantai fault (WQYF) against the North China craton (Fig. 1). The WQYF most likely represents the tectonic boundary between the North China and Yangtze cratons (e.g. Ernst et al. 2007). The metamorphic rocks of the Sulu UHP belt comprise granitic gneisses and quartzofeldspathic schists and minor kyanite-bearing quartzites, marbles, amphibolites and ultramafic rocks. Eclogites are hosted within all these lithologies and were mainly derived from continental tholeiites (Tang et al. 2007). The preservation of coesite and phengite in garnet, omphacite, kyanite or zircon and exsolution textures in olivine provide evidence that eclogites and country rocks were subjected to subduction at the leading edge of the Yangtze plate to depths exceeding 100–200 km (Ye et al. 2000a, b).

Whereas in the Dabie Shan post-orogenic magmatic activity was largely restricted to the Cretaceous (~130–112 Ma, Ma et al. 1998; Zhang et al. 2002), the Sulu belt records a more extended magmatic evolution comprising Triassic, Jurassic and Early Cretaceous granitoids (e.g. Guo et al. 2005; Liu et al. 2008). Triassic granitoids have so far only been reported from the Shidao igneous complex, situated at the easternmost Jiaodong peninsular, Shandong province (Fig. 2). Rocks of similar age or tectonic position occur outside the UHP terrane in the Qinling terrane (Sun et al. 2002) and at the northern and southern margin of the North China craton (northern and southern syenite belt according to Peng et al. 2008). A third, Late Triassic syenite belt can be traced onto the Korean peninsula, a possible extension of the Chinese Sulu terrane (Zhai et al. 2007b), but this belt has not yet been studied in detail (for a recent description of the Tokdal pluton, see Peng et al. 2008).

The Shidao igneous complex comprises two plutons – Jiazishan and Cashan (Fig. 2), which are mainly composed of pyroxene-syenites, quartz-syenites and granites (Chen et al. 2003). More mafic rock types, such as gabbro, occur in the southwestern part of the Jiazishan pluton close to its contact with the Cashan pluton.

The Shidao igneous complex has yielded important insight into subduction-related mantle enrichment processes and the composition of the lithospheric mantle (Gao et al. 2004; Yang et al. 2005). However, the exact origin of this complex is still controversial (Chen et al. 2003; Yang et al. 2005, 2006; Xie et al. 2006). Chen et al. (2003) suggested that the granitoids formed by partial melting of mantle material in response to break-off of the subducted Yangtze plate. According to this model, upwelling of hot asthenospheric mantle material triggered melting of the lithospheric mantle wedge between the subducted Yangtze slab and the North China craton. In contrast, Yang et al. (2005) argued that the melts were derived by partial melting of metasomatized subcontinental lithospheric mantle at the bottom of the Yangtze plate (i.e., they originated from the footwall craton). Whereas Nd and Sr isotope compositions cannot

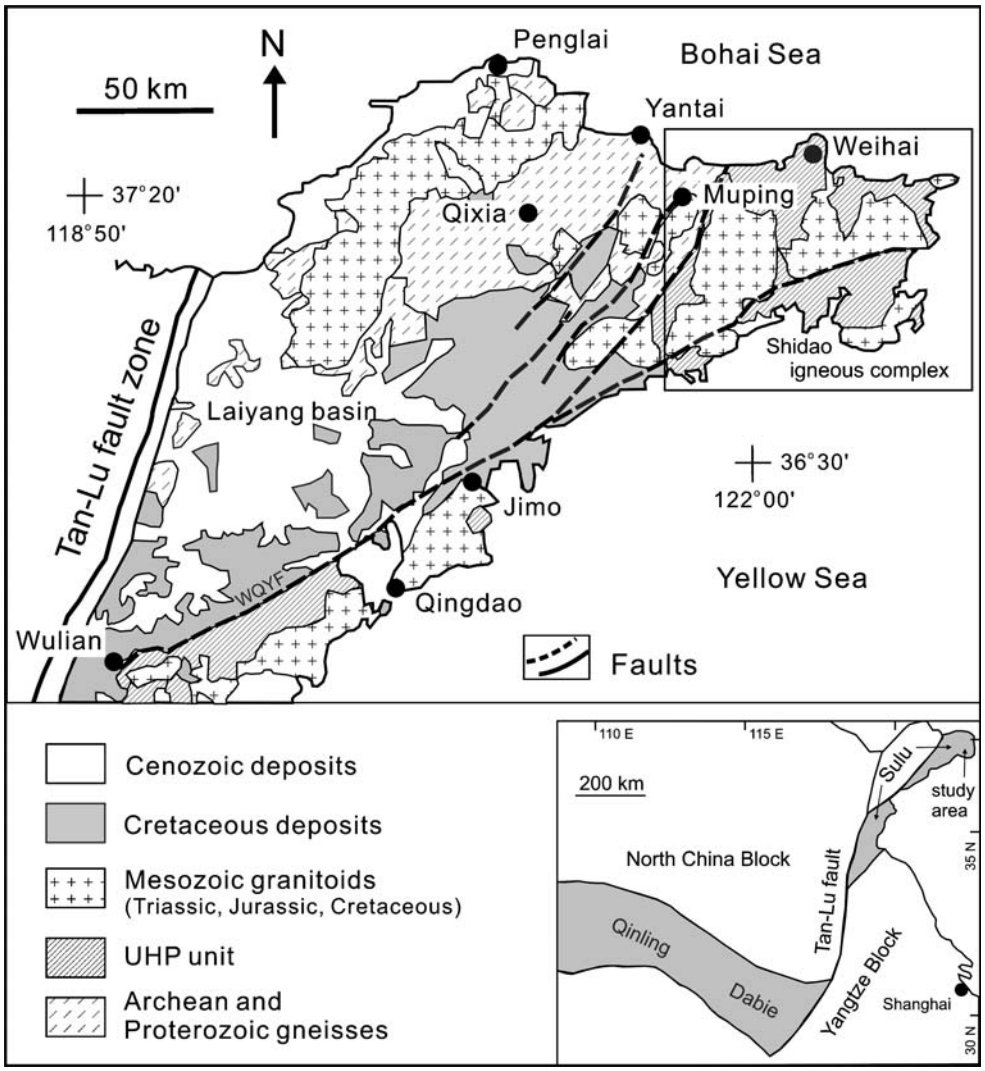

Fig. 1 Simplified geological map of the Jiaodong peninsular, eastern China. Inset map outlines extension of the Qinling-Dabi-Sulu metamorphic belt. WQYF = Wulian-Qingdao-Yantai fault

distinguish between the sources, Pb isotopic data seem to corroborate the model of Chen et al. (2003) and suggest that the source of the Shidao igneous complex was the lithospheric mantle beneath the North China craton (Xie et al. 2006).

Host rocks of the Shidao igneous complex are migmatitic granitic gneisses of the Sulu UHP terrane. At Moye Dao (Fig. 2) these rocks are well exposed and commonly strike northeast (*c*. 30°) and dip 50–60° to the southeast. The structural features are probably related to nappe thrusting during exhumation (Zhang et al. 2007). Although the northern and southern boundaries between the plutonic rocks and the granitic gneisses are narrow shear zones, it has been argued that the granitoids intruded into the UHP rocks (Guo et al. 2005).

Abundant zircon U-Pb age data exist on the syenitic rocks of the Shidao igneous complex: for pyroxene syenites U-Pb TIMS ages of 225±2 Ma (Chen et al. 2003) and SHRIMP ages of 212±1 Ma and 209±7 Ma (Guo et al. 2005) were reported. Quartz syenite samples were dated at 215±5 Ma (Yang et al. 2005, SHRIMP data), 211±3 Ma (Chen et al. 2003, U-Pb TIMS method), 212±2 Ma and 205±4 Ma (Guo et al. 2005 SHRIMP data). Hornblende from a pyroxene syenite yielded an $^{40}Ar/^{39}Ar$ plateau age of 214.6±0.6 Ma, indistinguishable from a $^{40}Ar/^{39}Ar$ K-feldspar age of 214.4±0.3 Ma from the same rock-type (Yang et al. 2005). Based on the geochronological data set, Yang et al. (2005) inferred an emplacement interval of *c*. 215–209 Ma for the syenites and concluded that the intrusion of the Jiazishan syenites closely postdated the UHP metamorphic peak (240–220 Ma).

Analytical techniques

Unless otherwise stated, analytical work was performed in the laboratories of the Institute of Geosciences, Tübingen University. Whole-rock and minerals separates (amphibole, pyroxene, biotite, titanite and apatite) were extracted from approximately 3 kg rock, using standard separation techni-

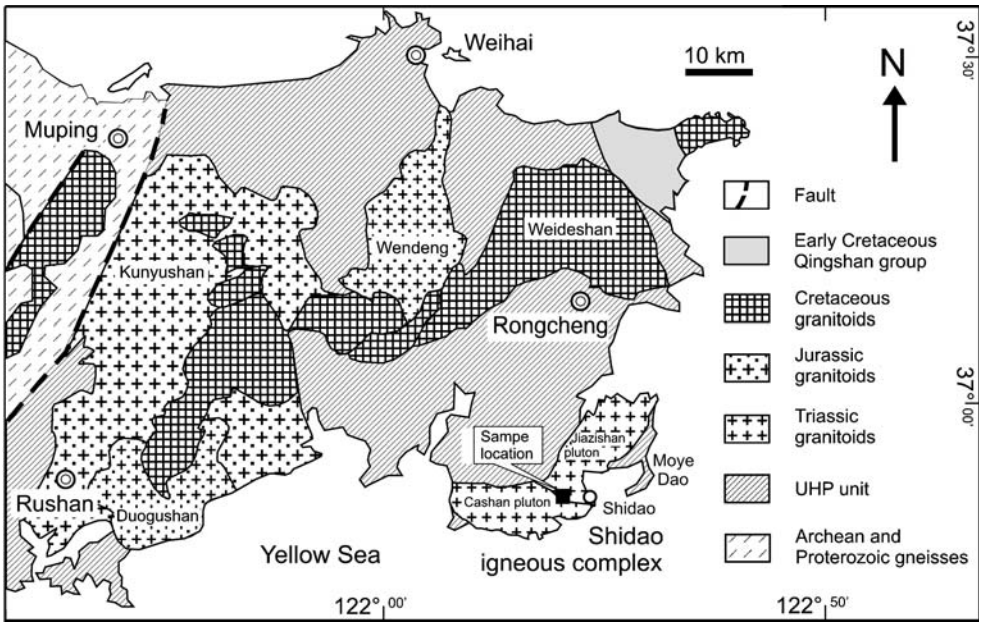

Fig. 2 Geological map of the eastern Sulu terrane, displaying distribution of UHP rocks, Mesozoic granites and sample location

ques. Major and trace element concentrations of whole-rock and minerals were determined by wavelength dispersive X-ray fluorescence (XRF) spectrometry on fused glass beads. Measurements were performed on a Bruker AXS S4 Pioneer spectrometer by standard analytical techniques (Potts and Webb 1992). Oxygen was extracted at 600°C from approximately 10 mg of dried mineral powder, employing BrF_5 as reagent and using a modified version of standard techniques (Clayton and Mayeda 1963). Oxygen was converted to CO_2 using a graphite rod heated by a Pt-coil and CO_2 was analysed for $^{18}O/^{16}O$ with a Finnigan MAT 251 gas source mass spectrometer. The isotopic ratios are reported in the δ-notation relative to Vienna standard mean ocean water (V-SMOW). The values represent the average of two analyses and analytical precision is better than ±0.2‰. $\delta^{18}O$ values of +9.72±0.2‰ and +9.61±0.2‰ ($2\sigma_m$) were obtained for the NBS–28 quartz standard and all data are normalized to the certified value of +9.64.

For Rb-Sr and Sm-Nd isotope analyses, mineral powders (<10 μm) were digested in 52% HF for four days at 140°C on a hot plate and spiked with mixed $^{87}Rb/^{84}Sr$ and ^{149}Sm-^{150}Nd tracer solutions. Rb, Sr, Sm and Nd were isolated by standard ion exchange chromatographic techniques. All isotopic measurements were made by Thermal Ionization Mass Spectrometry, on a Finnigan MAT 262 mass spectrometer in static mode. The $^{87}Sr/^{86}Sr$ and $^{143}Nd/^{144}Nd$ isotope ratios were normalised to $^{86}Sr/^{88}Sr=0.1194$ and to $^{146}Nd/^{144}Nd=0.7219$, respectively. Twelve replicate runs of the LaJolla Nd standard gave a $^{143}Nd/^{144}Nd$ ratio of 0.511867±0.000014 (2σ SD, reference value 0.511850) and the NBS 987 Sr standard yielded an $^{87}Sr/^{86}Sr$ ratio of 0.710266±0.000020 ($n=19$, 2σ SD, reference value 0.710240). Total procedural blanks (chemistry and loading) were <200 pg for Sr and <40 pg for Nd. $^{143}Nd/^{144}Nd$ ratios are quoted in the εNd notation as deviations from a chondritic reference (CHUR) with present-day $^{147}Sm/^{144}Nd$ and $^{143}Nd/^{144}Nd$ ratios of 0.1960 and 0.512630, respectively (Bouvier et al. 2008). External reproducibility was evaluated by analyses of twelve separate loads of granite G2 (USGS standard material), and the uncertainties (2σ SD) were 0.5% for $^{87}Rb/^{86}Sr$ and $^{147}Sm/^{144}Nd$ ratios, 0.03% for $^{87}Sr/^{86}Sr$ ratios and <0.001% for the $^{143}Nd/^{144}Nd$ ratios. Isochron calculation was performed using the Isoplot 3.0 software (Ludwig 2003).

For fission-track (FT) analysis, separated apatite and titanite crystals were embedded in epoxy and polished to 4π geometry. Spontaneous tracks in apatite were revealed by etching with 5.5 M HNO_3 solution for 20 s at 21°C (Donelick et al. 1999), and in titanite by etching with a solution of 1 HF : 2 HNO_3 : 3 HCl : 6 H_2O at 23°C for 6–30 min (Gleadow and Lovering 1974). FT dating was carried out using the external detector method (Gleadow 1981) with low-uranium muscovite sheets (Goodfellow mica™). The IUGS-recommended zeta calibration approach was taken for age determination (Hurford and Green 1983). Zeta values (Hurford 1998) of 306.3±4.8 (apatite) and 283.5±6.2 (titanite) for dosimeter glass CN-5 have been derived from 19 determinations of apatite and 6 of titanite from the Fish Canyon Tuff (apatite and titanite) and Durango (apatite). FT ages were calculated with TRACKKEY 4.1 (Dunkl 2002). Modeling of the low-temperature thermal history based on apatite fission-track data was carried out using the HeFTy modeling program (Ketcham 2005). A detailed description of analytical procedures is given in Danišík et al. (2008).

For (U-Th)/He analyses, apatite crystals were hand-picked following selection procedures described by Farley (2002). Each selected crystal was digitally photographed and measured in order to calculate the preliminary F_T-correction factor which considers the loss of helium in crystals of various geometries (Farley et al. 1996). Single crystals were loaded into Pt-tubes and heated by laser at ~800°C for 5 min after the complete line was evacuated to pressures < 9×10^{-8} mbar. Gas released from the crystals was purified and spiked with ^{3}He, and analysed by a quadrupole mass spectrometer (Pfeiffer Prisma QMS-200). ^{4}He/^{3}He ratios were measured by channeltron detector operated in static mode, and were corrected for HD and ^{3}H by monitoring mass 1. Absolute ^{4}He concentrations were calculated from peak height comparison against ratios of ^{4}He standards with known volume, measured before and after sample analysis. The analytical uncertainty on sample He determination was usually less than 2%. Following He measurements, the encapsulated crystals were analysed for U-Th at the Scottish Universities Environmental Research Centre (SUERC) in East Kilbride by VG PlasmaQuad 2 ICP-MS. U and Th content in the samples were accurate to ±2.5% (1σ). The total analytical uncertainty (TAU) was computed as a square root of sum of squares of weighted uncertainties on U, Th and He measurements. TAU was usually less than ~4% (1σ) and was used to calculate error of raw (U-Th)/He ages. The raw (U-Th)/He ages were corrected by F_T correction following Farley et al. (1996). The value of 5% was adopted as the uncertainty of F_T correction, and was used to calculate error of corrected (U-Th)/He ages. Replicate analyses of Durango apatite over the period of this study (30 analyses) yielded a mean (U-Th)/He age of 30.8 Ma with 1σ standard deviation of 2.5 Ma, which is in good agreement with reference (U-Th)/He age of 31.1±1.0 Ma (McDowell et al. 2005).

Results

Field observations and sample characterization

The sample studied here is a coarse-grained gabbro from the Yunmen locality, southwestern part of the Jiazishan pluton (Fig. 2). At this locality (36°52′39″N, 122°22′59″E), the gabbro forms an ellipsoidal body >100 m in diameter, and is overlain by pyroxene-syenite (Fig. 3a). The contact of the gabbro with the surrounding syenite is sharp but numerous dykes and veins of syenite anastomose through the gabbro (Fig. 3a), which suggests that the syenite intruded the gabbro when the latter was only partially consolidated. The gabbro displays a coarse-grained poikilitic texture with large biotite and plagioclase oikocrysts enclosing numerous crystals (i.e., chadacrysts) of pyroxene, amphibole and apatite (Fig. 3b–d). Except plagioclase, which is extensively replaced by sericite, other minerals are largely unaltered. Pyroxene and amphibole are abundant mafic phases (Fig. 3e) whereas olivine has not been observed. The gabbro contains a high proportion of apatite crystals (2–3%, Fig. 3f), the source of phosphate mining operations in the past. Titanite and iron sulfide are accessory phases.

Geochemistry and oxygen isotope data

Geochemical data for pyroxene, amphibole, biotite, apatite and whole-rocks are presented in Table 1. Concentration for Rb, Sr, Sm and Nd have been determined by isotope dilution; all others by XRF. Chemical analysis on plagioclase was not performed due to intense alteration and clustering of inclusions in this mineral. The alkaline whole-rock composition is characterized by low Al_2O_3 (9.2 wt.%) and high CaO (15.8 wt%) concentrations resulting in weight CaO/Al_2O_3 ratio of 1.7. The rock is shoshonitic with a K_2O/Na_2O ratio (by weight) of 1.6. The high total alkali content (Na_2O+K_2O=4.4 wt.%) and the position in the R1–R2 diagram (de la Roche et al. 1980, not shown) is compatible with an alkali-gabbro classification.

Dark mica shows strong pleochroism and, based on its molar Mg/Fe^{2+} ratio of 1.5, is Fe-Mg biotite. Pyroxenes show very low TiO_2 content (0.33 wt%) similar to those found in mantle xenocrysts (Wass 1979). The extreme source enrichment is well reflected in the geochemical composition of apatite which has high abundances of Sr (3307 ppm) and rare earth elements (La: 1545 ppm, Ce: 3648 ppm, Nd: 1652 ppm, Sm: 239 ppm, Yb: 25 ppm). Significant amounts of Zr occur in apatite (2162 ppm), as well as in amphibole (873 ppm). Whereas the rare earth element concentration of apatite is in the range reported for mantle apatite (O'Reilly and Griffin 2000), the Zr concentration is unexpectedly high. We cannot offer a satisfying explanation for this finding since no impurities in the apatite separate were identified. Ba is concentrated in biotite (10623 ppm) and, to a lesser extent, in apatite (784 ppm). The highest Nd and Sm concentrations were measured in titanite (3980 ppm and 702 ppm, respectively) and it can be assumed that this mineral, beside apatite, is a major carrier of the rare earth elements.

The oxygen isotope composition of the constituent minerals of the Jiazishan gabbro were determined in order to test if the $\delta^{18}O$ values provide evidence for mantle derivation, metasomatic processes and/or isotope equilibrium. Amphibole and pyroxene have $\delta^{18}O$ values (relative to V-SMOW) of 5.6‰ (Table 1), and are in the range of values found in rocks from mantle peridotites around the world (Mattey et al. 1994) and from the lithospheric mantle below northeastern China (Xu et al. 1996; Li et al. 1999b).

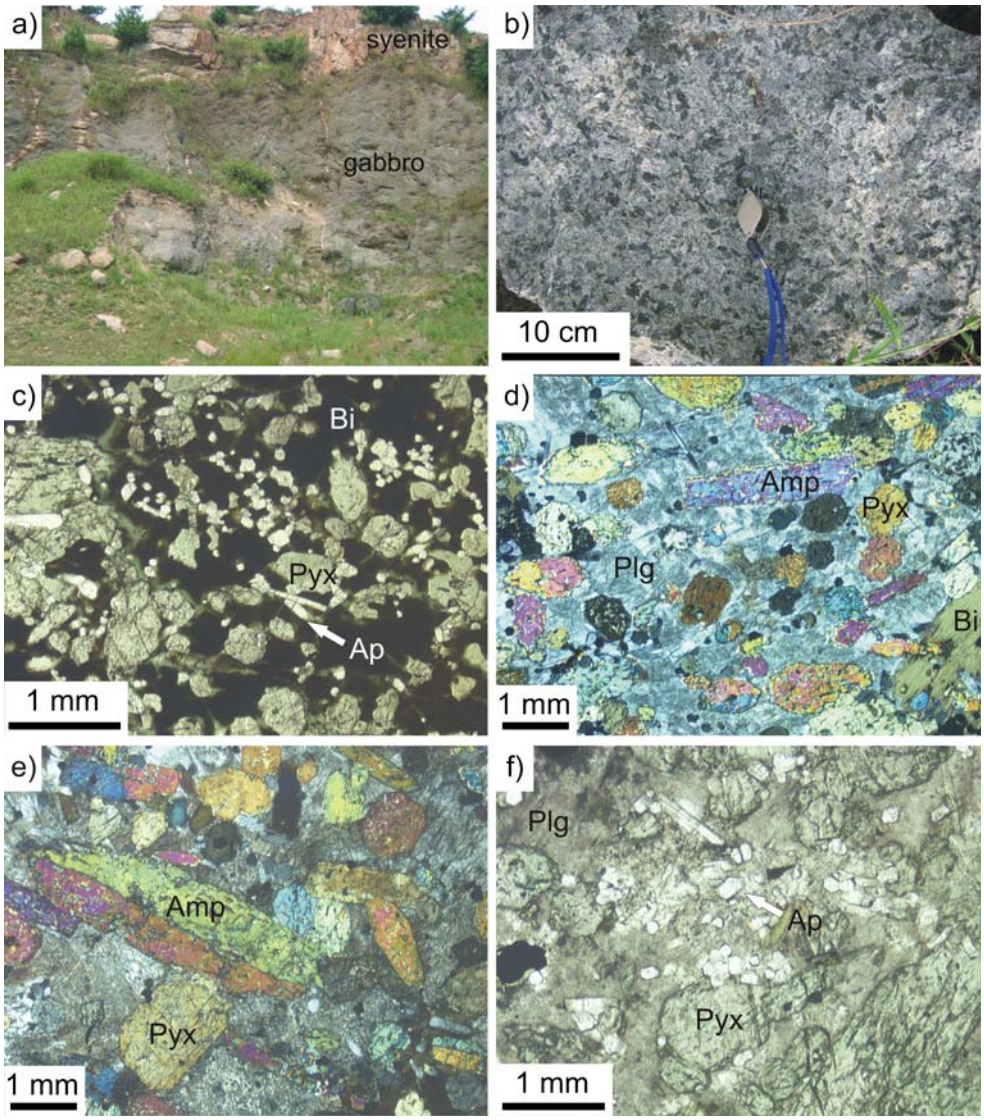

Fig. 3 **a** Field photograph of Jiazishan alkali-gabbro. At this locality the gabbro is overlain and intruded by veins and sheets of fine grained pyroxene-syenite; **b** Jiazishan gabbro boulder with regular distribution of large biotite oikocrysts; **c**–**f** photomicrographs of thin section from the Jiazishan gabbro (plane-polarized and crossed-nicols): **c** poikilitic texture defined by large crystals of biotite and **d** plagioclase; **e** zone with large crystals of (twinned) amphibole and pyroxene; **f** plagioclase oikocryst containing numerous apatite crystals. Abbreviations: Amp = amphibole, Ap = apatite, Bi = biotite, Plg = plagioclase, Pyx = pyroxene

We argue that the melt from which these minerals crystallized was in isotopic equilibrium with the mantle and that the amphibole and pyroxene minerals reflect this features of the source. Titanite is depleted in ^{18}O (4.1‰) compared to igneous titanite (King et al. 2001) and biotite is clearly depleted in ^{18}O (3.6‰) compared to mantle phlogopites (Ongley et al. 1987). This may indicate some oxygen isotope reequilibration of these minerals by a low $\delta^{18}O$ metasomatic fluid at high temperatures.

Sm-Nd and Rb-Sr data

Figure 4a shows the results of Sm-Nd analyses performed on apatite, biotite, titanite, pyroxene and amphibole from the Jiazishan gabbro. Due to strong sericitization neither plagioclase nor the whole-rock were analysed. Although the $^{147}Sm/^{144}Nd$ ratios are low and show narrow spread, the regression analyses yields a well defined isochron corresponding to an age of 226±36 Ma (2σ error, MSWD= 0.44) with an initial Nd isotope ratio of 0.511564±25 and an $\varepsilon Nd(t)$ value of −15.3 (Fig. 4a). The low initial εNd value is essentially the same as in the syenites (−16.5, Yang et al. 2005; −13.6 to −16.2, Gao et al. 2004) which reflects the isotope signature of the enriched lithospheric mantle below the North China craton (Chen et al. 2007; Liu et al. 2008). Rb-Sr analyses were carried out on biotite, amphibole, pyroxene and titanite. Since the latter three minerals plot close to the intercept of the regression line (0.706429±12), the resultant isochron age of 207±1 Ma (MSWD=1.7) is primarily defined by biotite (Fig. 4b).

Fission-track and (U-Th)/He data

Fission-track ages were successfully measured on titanite and apatite (Table 2). The titanite data passed the chi-square test at a 95% confidence interval and it is therefore

Table 1 Geochemical data for a whole-rock sample and extracted minerals from the Jiazishan gabbro (major elements in wt.% and trace elements in ppm)

	Whole-rock	Pyroxene	Amphibole	Biotite	Apatite	Titanite
SiO_2	47.93	50.67	45.52	33.79	2.55	
TiO_2	0.64	0.33	1.05	3.15	0.02	
Al_2O_3	9.22	1.87	4.65	15.56	0.61	
Fe_2O_3	7.32	8.94	12.97	19.03	0.27	
MnO	0.17	0.27	0.20	0.20	0.04	
MgO	9.07	13.44	16.32	14.48	0.19	
CaO	15.8	22.01	12.86	0.20	49.48	
Na_2O	1.66	0.65	1.51	0.16	0.35	
K_2O	2.71	0.10	0.49	7.40	0.17	
P_2O_5	2.79	0.17	0.31	0.02	47.39	
LOI	1.21	0.34	0.94	4.32	0.25	
Sum	98.52	98.79	96.82	98.31	101.32	
Ba	6326	103	81	10623	784	
Rb	72	2.3	2.2	315	–	1.4
Sr	2300	260	161	25	3307	310
V	162	191	304	521	43	
Y	48	15	–	–	291	
Zr	213	78	873	–	2162	
Zn	75	72	30	245	17	
Co	29	28	76	86	–	
Cr	92	106	59	223	–	
Ni	24	44	28	287	–	
La	184	130	125	–	1545	
Ce	295	223	–	–	3648	
Nd	142	44	47	0.21	1652	3980
Sm	19	8.6	9.0	0.04	239	702
Yb	4.9	1.1	2.0	–	25	
$\delta^{18}O$		5.6	5.6	3.6		4.1
$^{87}Rb/^{86}Sr$		0.0250	0.0390	37.584		0.0132
$^{87}Sr/^{86}Sr$ ($\pm 2\sigma_m$)		0.706512(7)	0.706528(9)	0.817305(10)		0.706474(10)
$^{147}Sm/^{144}Nd$		0.1184	0.1149	0.1056	0.0877	0.1066
$^{143}Nd/^{144}Nd$ ($\pm 2\sigma_m$)		0.511736(7)	0.511736(7)	0.511718(10)	0.511693(5)	0.511722(5)
εNd(t)		−15.3	−15.2	−15.3	−15.3	−15.3
T_{DM} (Ga)		2.24	2.23	2.24	2.24	2.24

LOI = loss on ignition; – below detection limit; $2\sigma_m$=2 sigma measured

εNd(t) refers to the initial (t=226 Ma) value

Depleded mantle model ages (T_{DM}) calculated after Liew and Hofmann (1988)

interpreted to form one age population and is reported as a central age with ±1 sigma error. The titanite fission-track age is 166±8 Ma. Track length distributions for apatite are unimodal, negatively skewed and relatively narrow (Fig. 5), with a mean confined track length of 13.1 μm and standard deviation of 1.3 μm (Table 2) that is typical of samples with moderate to fast cooling through the apatite partial annealing zone. The apatite yielded a mid-Cretaceous fission-track age of 106±6 Ma.

The single grain apatite (U-Th)/He ages corrected for alpha ejection range from 34±2 to 48±3 Ma with an average value of 39±5 Ma (Table 3). The replicates show good reproducibility and all are consistently younger than the corresponding apatite fission-track age.

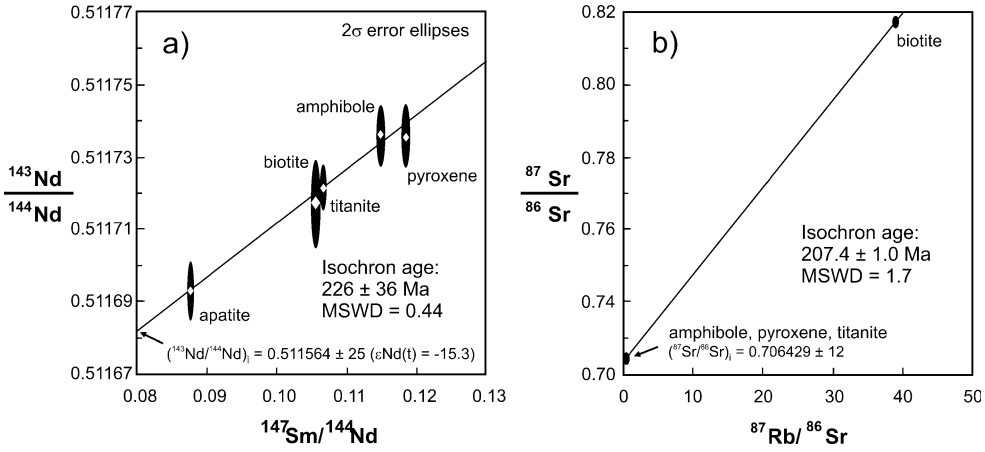

Fig. 4 **a** Sm-Nd mineral isochron diagram for apatite, biotite, titanite, amphibole and pyroxene; **b** Rb-Sr mineral isochron diagram for amphibole, pyroxene, titanite (all plotting close to the intercept of the regression line) and biotite

Discussion

The results from geochemistry and oxygen isotope analysis support the interpretation that the Jiazishan gabbro was derived by partial melting of a strongly enriched (metasomatized) subcontinental lithospheric mantle source which, as suggested previously, was generated by upflow and infiltration of melts and fluids from the subducted Yangtze plate (Yang et al. 2005, 2006; Xie et al. 2006). Syenites of this complex have identical isotopic compositions and share the same source (Yang et al. 2005). U-Pb zircon analyses show that the intrusion of the Shidao igneous complex occurred shortly after UHP metamorphism (Chen et al. 2003; Guo et al. 2005; Yang et al. 2005). Since the magmatic complex does not show evidence for high pressure overprinting, it can be assumed that a first phase of rapid exhumation of the UHP rock had proceeded to below UHP conditions at the time of magma emplacement. Evidence for fast obduction of the UHP terrane comes from the UHP rocks themselves. They show retrograde transformation into amphibolites. Dating of the retrograde mineral assemblage and low-pressure zircon rim domains suggests that the UHP rocks of the Sulu belt passed through high-pressure conditions at 216±3 Ma (Zhao et al. 2006). They experienced amphibolite retrogressive overprints at 211±4 Ma (Liu et al. 2004) and between 218 and 206 Ma (Liu et al. 2006), more or less simultaneous with formation of the Shidao igneous complex at *c*. 215–209 Ma (Yang et al. 2005). Although direct pressure estimates on the depth of crystallization for the Jiazishan intrusives are still lacking, this data suggest that at the time of intrusion, the UHP rocks in the Sulu area were exhumed to lower crustal levels (< 25 km).

The tectonic scenario outlined above is consistent with rapid cooling of the Shidao igneous complex. Rapid cooling is also indicated by the close correspondence between the syenite U-Pb zircon ages (*c*. 215–209 Ma, Chen et al. 2003; Guo et al. 2005; Yang et al. 2005), the syenite $^{40}Ar/^{39}Ar$ K-feldspar age (214–215 Ma, Yang et al. 2005) and the alkali-gabbro Rb-Sr biotite age (207±1 Ma, this study). Assuming a cooling rate of 20°/Ma the closure temperature of biotite for Sr diffusion is between 350–450° C (Giletti 1991; Jenkin et al. 2001). Thus we relate the Rb-Sr age of 207 Ma to exhumation of the Jiazishan gabbro to mid- to upper crustal levels. Onset of argon retention in K-feldspar occurs below 350°C (Lovera et al. 2002) whereas slow cooling rates would favour Ar loss in K-feldspar even below 125–175°C (i.e., at temperatures below the ~285–

Table 2 Fission-track data for apatite and titanite from Jiazishan gabbro

Sample code	N	ρs	Ns	ρi	Ni	ρd	Nd	P(χ2) (%)	Disp.	age (Ma)	± 1σ (Ma)	MTL (μm)	SD (μm)	N (L)	Dpar (μm)
apatite JZA	31	5.287	815	4.677	721	6.173	2801	>95	0.0	106.0	6.0	13.1	1.3	100	1.6
titanite JZT	25	86.991	1998	45.368	1042	6.196	2801	>95	0.0	166.2	8.0				

N number of dated apatite crystals, ρ_s (ρ_i) spontaneous (induced) track densities ($\times 10^5$ tracks/cm^2), N_s (N_i) number of counted spontaneous (induced) tracks, ρ_d dosimeter track density ($\times 10^5$ tracks/cm^2), N_d number of tracks counted on dosimeter, $P(\chi^2)$ probability obtaining Chi-square value (χ^2) for n degree of freedom (where *n*=No. of crystals − 1), *Disp*. dispersion, *age±1σ* − central age±1 standard error (Galbraith and Laslett 1993), *MTL* mean track length, *SD* standard deviation of track length distribution, *N* (*L*) number of horizontal confined tracks measured; D_{par} − average D_{par} values. Ages were calculated using zeta calibration method (Hurford and Green 1983), glass dosimeter CN-5, and zeta values of 306.3±4.8 and 283.5±6.2 year/cm^2 for apatite and titanite, respectively

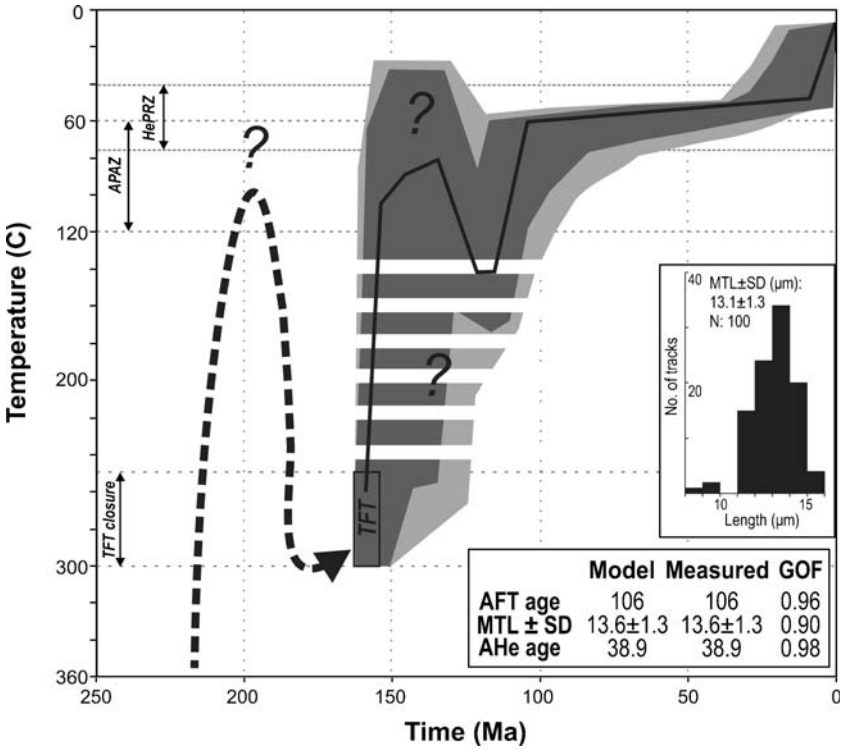

Fig. 5 Thermal modeling results of apatite helium (AHe), apatite fission track (AFT) and titanite fission track (TFT) data displayed in a time-temperature diagram modeled with HeFTy program (Ketcham 2005). Light gray envelopes indicate acceptable fit; dark gray envelopes indicate good fit; solid thick black line is the best fit; APAZ – apatite partial annealing zone; HePRZ – apatite helium partial retention zone; MTL is mean track length in μm; SD is standard deviation in μm; GOF is goodness of fit (statistical comparison of the measured input data and modeled output data, where a "good" result corresponds to value 0.5 or higher, "the best" result corresponds to value 1). *Inset*: Length distribution of the horizontal confined tracks in apatites

240°C closure temperature for fission-tracks in titanite). Since the $^{40}Ar/^{39}Ar$ K-feldspar age of Yang et al. (2005) exceeds the fission-track titanite age, we assume that the Jiazishan complex cooled rapidly below temperatures of 350°C.

The Jurassic titanite fission-track age (166±8 Ma) clearly post-dates the Triassic exhumation and cooling period. The large time gap between the titanite age and other mineral ages ($^{40}Ar/^{39}Ar$ K-feldspar, Rb-Sr biotite) indicates that the main driving parameters of exhumation such as buoyancy forces slowed down during the late Triassic and that the crust had probably reached post-orogenic thermal relaxation during the early Jurassic.

Along the Tan-Lu fault zone, detrital white micas from Triassic-Jurassic foreland sediments contain high Si contents, indicating initial exposure of high-pressure and even ultrahigh-pressure rocks in this part of the Sulu belt during the Middle Jurassic (Grimmer et al. 2003). If the Jiazishan gabbro was at upper crustal levels during the Jurassic, a reheating event is required to raise temperatures above the fission-track closure temperature of titanite (285–240°C). Reheating could be achieved by regional subsidence, for which there is no profound evidence during this period in the eastern Jiaodong peninsular. Alternatively, a thermal weakening or heat flow process could have increased the temperatures. In contrast to the Dabie area, the Sulu belt was affected by a widespread crustal melting event during the Jurassic. Jurassic granitoids in the eastern Jiaodong peninsular comprise the Duogushan (*c*. 160 Ma), Kunyushan and Wendeng (160–140 Ma) plutons (Guo et al. 2005) (Fig. 2). We conclude that these plutons, or unexposed portions of similar age, transported heat into the upper crust of the North China craton which led to annealing of the fission-tracks in titanite.

Apatite from the Jiazishan alkali-gabbro yields a Cretaceous fission-track age of 106±6 Ma. The grains show an asymmetric track length pattern indicating protracted cooling through the partial annealing zone (PAZ 120–60°C). During the Cretaceous, the geological situation on the eastern Jiaodong peninsula was dominated by the opening of pull-apart basins, deposition of the Early Cretaceous Qingshan group north of the study area (Fig. 2) and by nappe and shear zone activity lasting until 120 Ma (Zhang et al. 2007). There is clear evidence for lithospheric thinning and lower crustal delamination beneath the eastern North China craton during the Mesozoic (Kusky et al. 2007; Zhai et al. 2007a) and this process, which also affected the Sulu belt between 110 and 130 Ma (Liu et al. 2008), gave rise to volcanic and plutonic activity. The Weideshan pluton (108 ±2 Ma, Guo et al. 2005) is the nearest example of a Cretaceous igneous body in the eastern Sulu terrane, located only *c*. 40 km to the north of the Shidao igneous complex (Fig. 2). The thermal aureoles of such plutons, or unexposed equivalents of similar age, could have contributed to the reheating of the eastern Sulu terrane. From the apatite track length distribution we assume that the crust reached high enough temperatures to partially anneal fission-tracks in apatite (i.e., 60–120°C). It should be noted

Table 3 (U-Th)/He data for apatite crystals from Jiazishan gabbro

Sample code	N_c	Th (ng)	Th error (%)	U (ng)	U error (%)	^{4}He (ncc at STP)	^{4}He error (%)	TAU (%)	Th/U	Unc. age (Ma)	±1σ (Ma)	F_T	Cor. age (Ma)	±1σ (Ma)
JZA#1	1	0.344	2.3	0.045	4.3	0.472	1.0	2.8	7.61	30.8	0.9	0.76	40.8	2.3
JZA#3	1	0.757	1.6	0.100	2.0	0.899	1.0	1.9	7.59	26.6	0.5	0.79	33.5	1.8
JZA#5	1	0.726	2.4	0.120	2.2	1.277	1.0	2.6	6.05	36.1	0.9	0.82	43.9	2.5
JZA#6	1	0.751	2.3	0.113	3.5	0.846	1.0	2.6	6.67	24.1	0.6	0.81	29.6	1.7
JZA#7	1	0.411	1.7	0.054	3.1	0.580	1.0	2.2	7.68	31.7	0.7	0.76	41.6	2.3
JZA#9	1	0.597	2.2	0.128	2.8	0.997	1.0	2.5	4.66	30.5	0.8	0.80	38.2	2.1
JZA#11	1	0.890	2.4	0.149	2.8	1.778	1.0	2.6	5.99	40.8	1.1	0.85	47.9	2.7
JZA#12	1	0.903	2.0	0.155	2.2	1.539	1.0	2.2	5.82	34.4	0.8	0.83	41.5	2.3
JZA#15	1	0.868	2.2	0.111	2.9	1.086	1.0	2.5	7.82	28.3	0.7	0.81	34.8	1.9
JZA#16	1	1.053	2.2	0.150	2.8	1.651	1.0	2.5	7.02	34.1	0.9	0.84	40.8	2.3
JZA#20	1	0.822	2.3	0.148	3.2	1.254	1.0	2.7	5.55	30.2	0.8	0.86	35.3	2.0
Average (Ma)													38.9	5.2
Std. dev. (Ma)														

N_c number of dated apatite crystals, *TAU* total analytical uncertainty, *Unc. age* uncorrected AHe age, F_T alpha recoil correction factor after Farley et al. (1996)

that Cretaceous heating was very pronounced in the Dabie Shan zone where presently exposed rocks were subjected to temperatures >300°C (North Dabie basement, Ratschbacher et al. 2000) and >200°C (South Dabie basement, Grimmer et al. 2002). Thus, Cretaceous reheating was much weaker in the eastern Sulu belt than in the Dabie Shan and this is also corroborated by the fact that the fission-tracks in titanite were not affected by this event.

In order to reveal the thermal history of the Jiazishan alkali-gabbro, consistent with measured apatite fission-track and apatite helium data, we used the HeFTy modeling program (Ketcham 2005). This program provides potential thermal pathways by combining the fission-track annealing and He diffusion-production models. Several values for the titanite fission-track closure temperature have been reported (e.g. 250±50°C: Gleadow and Brooks 1979; 240±40°C: Harrison et al. 1979; 275±25°C: Fitzgerald and Gleadow 1988; 275±25°C: Kohn et al. 1993; 265–310°C: Coyle and Wagner 1998; 285°C: Jacobs and Thomas 2002), in this study we adopt the value of 275±25°C following Fitzgerald and Gleadow (1988) and Kohn et al. (1993). We constrained the model using the known titanite fission-track age (158–164 Ma) and modeled time-temperature paths in the "unsupervised search style", employing a Monte Carlo searching algorithm with 100,000 iterations. The analysed sample reveals a time-temperature path with an episodic cooling history (Fig. 5) that can be characterized as follows: the time-temperature path starts with the cooling from the titanite closure temperature levels to the apatite partial annealing zone lasting from ~160 to ~140 Ma. The following temperature increase to >120°C at ~120 Ma likely represents a reheating event associated with magmatic activity known from geological evidence given above. Subsequent short cooling phase at ~110 Ma is followed by a period of thermal stagnation or landscape stability evidenced by long residence within the temperature range of ~50–75°C starting at ~100 Ma. The onset of final accelerated cooling, which led to the present exposure of the Sulu belt, started earliest at ~25 Ma as suggested by the thermal modelling results.

Conclusions

The Shidao igneous complex intruded the UHP rocks after a stage of ultra-fast exhumation. The rocks were transported towards the surface, sandwiched between the UHP units, by a multistage unroofing process. Sm-Nd and Rb-Sr mineral ages of the Jiazishan alkali-gabbro and previously published U-Pb and $^{40}Ar/^{39}Ar$ mineral ages of the syenites support the model of rapid exhumational cooling of the granitoids after emplacement into the UHP crust. Cooling slowed down remarkably at the end of the Triassic when the UHP rocks resided in upper crustal levels. Titanite and apatite fission-track ages record episodes of reheating during Jurassic and Cretaceous granitoid magmatism, respectively. During the Jurassic igneous event the Jiazishan gabbro was reheated above the fission-track annealing temperatures of titanite (>250–280°C). Cretaceous magmatism and lithospheric thinning thermally weakened the crust for a second time and this event, recorded in the apatite fission-track data (106±6 Ma), was associated with further uplift and erosion. An interval of thermal stability of *c*. 50 Ma prevailed from late Cretaceous to early Tertiary

times. This was followed by a final phase of accelerated unroofing during late Eocene that lasted until the present day.

Acknowledgements We are grateful to Gisela Bartholomä, Elmar Reitter, Bernd Steinhilber, Gabriele Stoscheck and Heiner Taubald for analytical help during sample preparation and isotope analyses and to Noreen Evans for U-Th analyses and English language corrections.

References

Ames L, Tilton GR, Zhou GZ (1993) Timing of collision of the Sino-Korean and Yangtze cratons: U-Pb zircon dating of coesite-bearing eclogites. Geology 21:339–342

Ayers JC, Dunkle S, Gao S, Miller CF (2002) Constraints on timing of peak and retrograde metamorphism in the Dabie Shan ultrahigh-pressure metamorphic belt, east-central China, using U-Th-Pb dating of zircon and monazite. Chem Geol 186:315–331

Bouvier A, Vervoort JD, Patchett PJ (2008) The Lu-Hf and Sm-Nd isotopic composition of CHUR: constraints from unequilibrated chondrites and implications for the bulk composition of terrestrial planets. Earth Planet Sci Lett 273:48–57

Chen JF, Xie Z, Li HM, Zhang XD, Zhou TX, Park YS, Ahn KS, Chen DG, Zhang X (2003) U-Pb-zircon ages for a collision-related K-rich complex at Shidao in the Sulu ultrahigh pressure terrane, China. Geochem J 37:35–46

Chen B, Zhai MG, Tian W (2007) Origin of the Mesozoic magmatism in the North China craton: constraints from petrological and geochemical data. In: Zhai MG, Windley BF, Kusky TM, Meng QR (eds) Mesozoic sub-continental lithospheric thinning under eastern Asia. Geol Soc London, Spec Publ 280, pp 131–151

Clayton RN, Mayeda TK (1963) The use of bromine pentafluoride in the extraction of oxygen from oxides and silicates for isotopic analysis. Geochim Cosmochim Acta 27:43–52

Coyle DA, Wagner GA (1998) Positioning the titanite fission-track partial annealing zone. Chem Geol 149:117–125

Danišík M, Sachsenhofer RF, Privalov VA, Panova EA, Frisch W, Spiegel C (2008) Low-temperature thermal evolution of the Azov Massif (Ukrainian Shield - Ukraine) - implications for interpreting (U-Th)/He and fission track ages from cratons. Tectonophysics 456:171–179

de la Roche H, Leterrier J, Grand Claude P, Marchal M (1980) A classification of volcanic and plutonic rocks using R1–R2 diagrams and major element analyses—its relatioship with current nomenclature. Chem Geol 29:183–210

Donelick RA, Ketcham RA, Carlson WD (1999) Variability of apatite fission-track annealing kinetics: II. Crystallographic orientation effects. Am Mineral 84:1224–1234

Dunkl I (2002) TRACKKEY: a Windows program for calculation and graphical presentation of fission track data. Comput Geosci 28:3–12

Ernst WG, Tsujimori T, Zhang R, Liou JG (2007) Permo-Triassic collision, subduction-zone metamorphism, and tectonic exhumation along the East Asian continental margin. Annu Rev Earth Planet Sci 35:73–110

Farley KA (2002) (U-Th)/He dating: techniques, calibrations, and applications. Mineral Soc Am Rev Mineral Geochem 47:819–844

Farley KA, Wolf RA, Silver LT (1996) The effects of long alpha-stopping distances on (U-Th)/He dates. Geochim Cosmochim Acta 60:4223–4229

Fitzgerald PG, Gleadow AJW (1988) Fission-track geochronology, tectonics and structure of the Transantarctic Mountains in northern Victoria Land, Antarctica. Chem Geol 73:1497–1502

Galbraith RF, Laslett GM (1993) Statistical models for mixed fission track ages. Nucl Tracks Radiat Meas 21:459–470

Gao TS, Chen JF, Xie Z, Yan J, Qian H (2004) Geochemistry of Triassic igneous complex at Shidao in the Sulu UHP metamorphic belt. Acta Petrologica Sinica 20:1025–1038 (in Chinese with English abstract)

Giletti BJ (1991) Rb and Sr diffusion in alkali feldspars, with implications for cooling histories of rocks. Geochim Cosmochim Acta 55:1331–1343

Gleadow AJW (1981) Fission track dating methods: what are the real alternatives? Nucl Tracks Radiat Meas 5:3–14

Gleadow AJW, Brooks C (1979) Fission-track dating, thermal histories and tectonics of igneous intrusions in east Greenland. Contrib Mineral Petrol 71:45–60

Gleadow AJW, Lovering JF (1974) The effect of weathering on fission track dating. Earth Planet Sci Lett 22:163–168

Grimmer JC, Jonckheere R, Enkelmann E, Ratschbacher L, Hacker BR, Blythe AE, Wagner GA, Wu Q, Liu S, Dong S (2002) Cretaceous-Cenozoic history of the southern Tan-Lu fault zone: apatite fission-track and structural constraints from the Dabie Shan (eastern China). Tectonophysics 359:225–253

Grimmer JC, Ratschbacher L, McWilliams M, Franz L, Gaitzsch I, Tichomirowa M, Hacker BR, Zhang Y (2003) When did the ultrahigh-pressure rocks reach the surface? A $^{207}Pb/^{206}Pb$ zircon, $^{40}Ar/^{39}Ar$ white mica, Si-in-white-mica, single-grain provenance study of Dabie Shan synorogenic foreland sediments. Chem Geol 197:87–110

Guo J, Chen F, Zhang X, Siebel W, Zhai M (2005) Evolution of syn- to post-collisional magmatism from north Sulu UHP belt, eastern China: zircon U-Pb geochronology. Acta Petrologica Sinica 21:1281–1301

Harrison TM, Armstrong RL, Naeser CW, Harakal JE (1979) Geochronology and thermal history of the Coastal plutonic complex, near Prince Rupert, British Columbia. Can J Earth Sci 16:400–410

Hurford AJ (1998) ZETA: the ultimate solution to fission-track analysis calibration or just an interim measure. In: Van den Haute P, de Corte F (eds) Advances in fission-track geochronology. Kluwer Academic, Dordrecht, pp 19–32

Hurford AJ, Green PF (1983) The zeta age calibration of fission-track dating. Chem Geol 41:285–312

Jacobs J, Thomas RJ (2002) A titanite fission track profile across the southeastern Archean Kaapvaal craton and the Mesoproterozoic Natal metamorphic province, South Africa: evidence for differential cryptic Meso- to Neoproterozoic tectonism. J Afr Earth Sci 33:323–333

Jenkin GRT, Ellam RM, Rogers G, Stuart FM (2001) An investigation of closure temperature of the biotite Rb-Sr system: the importance of cation exchange. Geochim Cosmochim Acta 65:1141–1160

Ketcham RA (2005) Forward and inverse modeling of low-temperature thermochronometry data. In: Reiners PW, Ehlers TA (eds) Low-temperature thermochronology: techniques, interpretations, and applications. Reviews in Mineralogy and Geochemistry 58, pp. 275–314

King EM, Valley JW, Davis DW, Kowallis BJ (2001) Empirical determination of oxygen isotope fractionation for titanite with respect to zircon and quartz. Geochim Cosmochim Acta 65:3165–3175

Kohn BP, Wagner ME, Lutz TM, Organist G (1993) Anomalous Mesozoic thermal regime, central Appalachian Piedmont: evidence from sphene and zircon fission-track dating. J Geol 101:779–794

Kusky TM, Windley BF, Zhai MG (2007) Lithospheric thinning in eastern Asia; constraints, evolution, and tests of models. In: Zhai MG, Windley BF, Kusky TM, Meng QR (eds) Mesozoic sub-

continental lithospheric thinning under eastern Asia. Geol Soc London, Spec Publ 280, pp 331–343

Li SG, Xiao Y, Liu D, Chen Y, Ge N, Zhang Z, Sun SS, Cong BL, Zhang R, Hart SR, Wang S (1993) Collision of the North China and Yangtze block and formation of coesite-bearing eclogites: Timing and processes. Chem Geol 109:89–111

Li SG, Jagoutz E, Lo CH, Chen Y, Li Q, Xiao Y (1999a) Sm/Nd, Rb/Sr and $^{40}Ar/^{39}Ar$ isotopic systematic of the ultrahigh-pressure metamorphic rocks in the Dabie-Sulu belt, central China: A retrospective view. Intern Geol Rev 41:1114–1124

Li Y, Wiechert U, Zheng YF, Zhi XC, Hoefs J (1999b) Laserprobe oxygen isotope analysis of minerals from mantle derived rocks in eastern China. Chinese Sci Bull 44:740–744

Li SG, Jagoutz E, Chen Y, Li Q (2000) Sm-Nd and Rb-Sr isotopic chronology and cooling history of ultrahigh pressure metamorphic rocks and their country rocks at Shuanghe in the Dabie orogen, central China. Geochim Cosmochim Acta 64:1077–1093

Liew TC, Hofmann AW (1988) Precambrian crustal components, plutonic associations, plate environment of the Hercynian fold belt of central Europe: indications from a Nd and Sr isotopic study. Contrib Mineral Petrol 98:129–138

Lin JQ, Tan DJ, Chi XG, Bi LJ, Xie CF, Xu WL (1992) Mesozoic granites in the Jiao-Liao Peninsula. Science, Beijing, 208 pp, in Chinese with English abstract

Liu J, Xu Z, Liou JG, Song B (2004) SHRIMP U-Pb ages of ultrahigh-pressure and retrograde metamorphism of gneisses, south-western Sulu terrane, eastern China. J Metamorph Geol 22:315–326

Liu FL, Gerdes A, Liou JG, Xue H, Liang FH (2006) SHRIMP U-Pb zircon dating from dolomitic marble, Sulu-Dabie terrane: restriction on the prograde, UHP and retrograde metamorphic ages. J Metamorphic Geol 24:569–589

Liu FL, Gerdes A, Robinson P, Xue HM, Ye JG (2007) Zoned zircon from eclogite lenses in marbles from the Dabie-Sulu UHP terrane, China: A unique record of ultra-deep subduction and fast exhumation. Acta Geol Sinica 81:204–225

Liu S, Hu R, Gao S, Feng C, Qi Y, Wang T, Feng G, Coulson IM (2008) U-Pb zircon age, geochemical and Sr-Nd-Pb-Hf isotopic constraints on age and origin of alkaline intrusions and associated mafic dikes from Sulu orogenic belt, eastern China. Lithos 106:365–379

Lovera OM, Grove M, Harrison TM (2002) Systematic analysis of K-feldspar $^{40}Ar/^{39}Ar$ step heating results II: relevance of laboratory argon diffusion properties to nature. Geochim Cosmochim Acta 66:1235–1255

Ludwig KR (2003) Isoplot/Ex, rev 3.00: A geochronological toolkit for Microsoft Excel. Berkeley Geochronology Center, Spec Publ No. 4, 1–58

Ma C, Li Z, Ehlers C, Yang K, Wang R (1998) A post-collisional magmatic plumbing system: Mesozoic granitoid plutons from the Dabieshan high-pressure and ultra-high pressure metamorphic zone, east-central China. Lithos 45:431–456

Mattey D, Lowry D, Macpherson C (1994) Oxygen isotope composition of mantle peridotite. Earth Planet Sci Lett 128:231–241

McDowell FW, McIntosh WC, Farley KA (2005) A precise ^{40}Ar-^{39}Ar reference age for the Durango apatite (U–Th)/He and fission-track dating standard. Chem Geol 214:249–263

Okay AI, Xu S, Şengör AMC (1989) Coesite from the Dabie Shan eclogites, central China. Eur J Mineral 1:595–598

Ongley J, Basu AR, Kyser TK (1987) Oxygen isotopes in coexisting garnets, clinopyroxenes and phlogopites of Roberts Victor eclogites: implications for petrogenesis and mantle metasomatism. Earth Planet Sci Lett 83:80–84

O'Reilly SY, Griffin WL (2000) Apatite in the mantle: implications for metasomatic processes and high heat production in Phanerozoic mantle. Lithos 53:217–232

Peng P, Zhai MG, Guo JH, Zhang HF, Zhang YB (2008) Petrogenesis of Triassic postorogenic syenite plutons in the Sino-Korean craton: an example from North Korea. Geol Mag 145:637–647

Potts PJ, Webb PC (1992) X-ray fluorescence spectrometry. J Geochem Explor 4:251–296

Ratschbacher L, Hacker BR, Webb LE, McWilliams M, Ireland T, Dong S, Calvert A, Chateigner D, Wenk HR (2000) Exhumation of the ultrahigh-pressure continental crust in east central China: Cretaceous and Cenozoic unroofing and the Tan-Lu fault. J Geophys Res 105:13303–13338

Sun WD, Li SG, Chen YD, Li YJ (2002) Timing of synorogenic granitoids in the South Qinling, central China: constraints on the evolution of the Qinling-Dabie orogenic belt. J Geol 110:457–468

Tang HF, Liu CQ, Nakai S, Orihashi Y (2007) Geochemistry of eclogites from the Dabie-Sulu terrane, eastern China: new insights into protoliths and trace element behaviour during UHP metamorphism. Lithos 95:441–457

Wang XM, Liou JG, Mao HK (1989) Coesite-bearing ecologite from the Dabie Mountains in central China. Geology 17:1085–1088

Wass SY (1979) Multiple origin of clinopyroxenes in alkali basaltic rocks. Lithos 12:115–132

Webb LE, Hacker BR, Ratschbacher L, McWilliams MO, Dong S (1999) Thermo-chronological constraints on deformation and cooling history of high- and ultrahigh-pressure rocks in the Qinling-Dabie orogen, eastern China. Tectonics 18:621–638

Xie Z, Li QZ, Gao TS (2006) Comment on "Petrogenesis of post-orogenic syenites in the Sulu orogenic belt, east China: geochronological, geochemical and Nd-Sr isotopic evidence" by Yang et al. Chem Geol 235:191–194

Xu S, Okay AI, Ji S, Şengör AMC, Su W, Liu Y (1992) Diamond from the Dabie Shan metamorphic rocks and its implication for tectonic setting. Science 256:80–82

Xu YG, Menzies MA, Mattey DP, Lowry D, Harte B, Hinton RW (1996) The nature of the lithospheric mantle near the Tancheng–Lujiang fault, China: an integration of texture, chemistry and O-isotopes. Chem Geol 134:67–81

Yang JH, Chung SL, Wilde SA, Wu FY, Chu MF, Lo CH, Fan HR (2005) Petrogenesis of post-orogenic syenites in the Sulu orogenic belt, east China: geochronological, geochemical and Nd-Sr isotopic evidence. Chem Geol 214:99–125

Yang JH, Chung SL, Wilde SA, Wu FY, Chu MF, Lo CH, Fan HR (2006) "Petrogenesis of post-orogenic syenites in the Sulu orogenic belt, east China: geochronological, geochemical and Nd-Sr isotopic evidence"–reply. Chem Geol 235:186–190

Ye K, Yao YP, Katayama I, Cong B, Wang QC, Maruyama S (2000a) Large areal extent of ultrahigh-pressure metamorphism in the Sulu ultrahigh-pressure terrane of East China: new implications from coesite and omphacite inclusions in zircon and granitic gneiss. Lithos 52:157–164

Ye K, Ye DN, Cong B (2000b) The possible subduction of continental material to depth greater than 200 km. Nature 407:734–736

Zhai MG, Fan QC, Zhang HF, Sui JL, Shao J (2007a) Lower crustal processes leading to Mesozoic lithospheric thinning beneath eastern North China: underplating, replacement and delamination. Lithos 96:36–54

Zhai MG, Guo JG, Li Z, Chen DZ, Peng P, Li TS, Hou Q, Fan QC (2007b) Linking the Sulu UHP belt to the Korean peninsula: evidence from eclogite, Precambrian basement, and Paleozoic sedimentary basins. Gondwana Res 12:388–403

Zhang HF, Gao S, Zhong Z, Zhang B, Zhang L, Hu SH (2002) Geochemical and Sr-Nd-Pb isotopic compositions of Cretaceous granitoids: constraints on tectonic framework and crustal structure of the Dabieshan ultrahigh-pressure metamorphic belt, China. Chem Geol 186:281–299

Zhang HY, Hou QL, DY CAO (2007) Study of thrust and nappe tectonics in the eastern Jiaodong peninsula, China. Sci China Ser D-Earth Sci 50:161–171

Zhao ZF, Zheng YF, Gao TS, Wu YB, Chen B, Chen FK, Wu FY (2006) Isotopic constraints on age and duration of fluid-assisted high-pressure eclogite-facies recrystallization during exhumation of deeply subducted continental crust in the Sulu orogen. J Metamorphic Geol 24:687–702

Zheng YF, Fu B, Gong B, Li L (2003) Stable isotope geochemistry of the ultrahigh pressure metamorphic rocks from the Dabie–Sulu belt in China: implications for geodynamics and fluid regime. Earth-Sci Rev 1276:1–57